Nanoporous Photocathode and Photoanode Made by Multilayer Assembly of Quantum Dots

Mohamad Hojeij, Bin Su, Shuxin Tan, Guillaume Me#riguet, and Hubert H. Girault

More About This Article

Additional resources and features associated with this article are available within the HTML version:

- Supporting Information
- Access to high resolution figures
- Links to articles and content related to this article
- Copyright permission to reproduce figures and/or text from this article

View the Full Text HTML

Nanoporous Photocathode and Photoanode Made by Multilayer Assembly of Quantum Dots

Mohamad Hojeij, Bin Su, Shuxin Tan, Guillaume Mériguet, and Hubert H. Girault*

Laboratoire d'Electrochimie Physique et Analytique, Ecole Polytechnique Fédérale de Lausanne, Station 6, CH-1015 Lausanne, Switzerland

ABSTRACT We perform in this paper a kinetic study of the photoelectrochemical responses of nanoporous thin photoactive films. The films were fabricated by by a layer-by-layer assembly of positively charged polyelectrolytes (poly-L-Lysine, pLys) and negatively charged semiconductor nanoparticles (NPs) on a carboxylic acid terminated alkanethiol-modified gold electrode. Two types of NPs were used to build uniform films: cadmium selenide (CdSe) and cadmium selenide/cadmium sulfide core/shell (CdSe@CdS). Large photocathodic and photoanodic currents were recorded for CdSe and CdSe@CdS sensitized films, respectively. A theoretical model of the photocurrent responses was developed to analyze the kinetics of photoinduced processes and coupled reactions, showing that the multilayer films behave as homogeneous nanoporous semiconducting photoelectrodes.

Semiconducting nanoparticles (NPs) represent an advanced dimension of materials that bridges bulk material and molecular behavior and offers prospects of novel and size-dependent optical, electronic, and optoelectric properties.[1–7] Extensive studies have been carried out to organize semiconducting NPs into thin films, for example by Langmuir–Blodgett (LB) techniques and by self-assembly methods.[8–13] The well-established layer-by-layer (LBL) assembly technique, initially developed for pairs of oppositely charged polyelectrolytes, has also been successfully employed.[14–22] The protocol is based on the electrostatic interactions between sequentially adsorbed monolayers of NPs and oppositely charged polyelectrolytes. It provides a simple and facile route to fabricate hybrid thin film structures. Incorporation of various types of semiconducting NPs has been reported, and the photocurrent generation at films thus formed has also been investigated.[12,17,23–26] In comparison with the monolayer film structures, a large amount of photoactive centers can be uploaded, and therefore a larger light harvesting can be obtained.

On the other hand, to optimize the assembly performance, it is important to understand how the electron transfer induced by light excitation proceeds through the film. Kotov *et al.* have reported photocurrent measurements at multilayers constructed from titanium dioxide (TiO_2) NPs and poly-(diallyldimethylammonium) (PDADMA) polyelectrolytes. It was shown that the photocurrent increases with increasing number of bilayers and reaches a maximum at 10 bilayers.[12] A similar trend has been observed later by Halaoui for multilayer films of cadmium sulfide (CdS) NPs and PDADMA.[25,26] The electron transport through the film was proposed to occur *via* electron hopping between the CdS NPs. In a recent publication, we have reported the photocurrent responses of hydrophilic ultrathin aqueous films composed of alternate layer of poly-Lysine (pLys) and poly-Glutamic acid (pGlu), sensitized by a terminal layer of CdSe NPs and placed in a water immiscible organic electrolyte solution.[17] The photoinduced electron transport through the film was shown to proceed mostly *via* electron hopping between the ferri/ferrocyanide mediators incorporated in the aqueous films. It has also been suggested in this study that the potential drop at the electrode takes place over about five polyelectrolyte bilayers.

The present work aims at constructing aqueous multilayer assemblies, (pLys/CdSe)$_n$, and (pLys/CdSe@CdS)$_n$, in which the NPs function both as a sensitizer and a mediator (Scheme 1). Electrostatic interactions between the positively charged pLys and the negatively charged NPs enables the build-up of multilayer films, as confirmed by optical spectroscopic measurements. The photoinduced carrier dynamics of CdSe and CdSe@CdS NPs in the films is studied by time-correlated single photon counting

*Address correspondence to hubert.girault@epfl.ch.

(TCSPC). It shows that the fluorescence decay of the NPs inside the film differs from that in aqueous solutions, indicating a longer lifetime when attached to the film. The photocurrent responses from multilayer films of different thicknesses are obtained in 1,2-dichloroethane (DCE) electrolyte solution. Photocathodic currents were mainly observed for $(pLys/CdSe)_n$ films and photoanodic currents were mainly recorded for $(pLys/CdSe@CdS)_n$ films. The dependences of photocurrent magnitude on the applied potential and the thickness of the film were quantitatively analyzed with a kinetic model of photoinduced charge transfer reactions. It is shown that the current increases with increasing film thicknesses, and is directly proportional to the number of the NPs layers. The rate constant of photoinduced reduction of CdSe and photoinduced oxidation and CdSe@CdS NPs at the gold electrode was found to depend on the applied potential and to be insensitive to the film thickness.
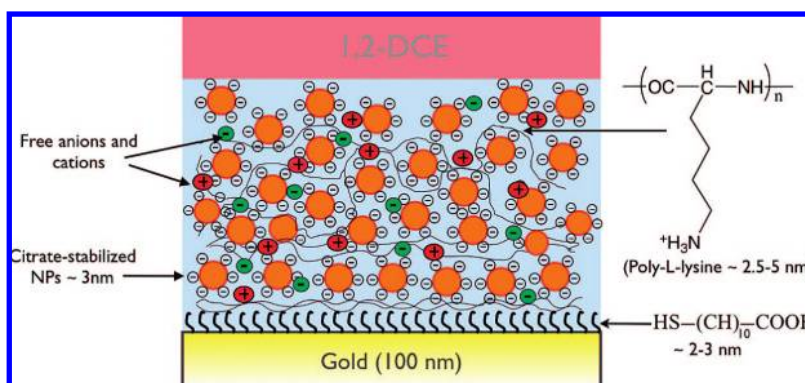

Scheme 1. Schematic representation of the ultrathin film $(pLys/NPs)_n$ assembled on MUA-modified-gold substrate.

RESULTS AND DISCUSSIONS

Characterization of the Growth of $(pLys/NPs)_n$ Multilayers. The growth of the alternating pLys/NPs composite multilayer film was monitored by UV−visible absorption and steady-state fluorescence spectroscopic measurements. Figure 1 panels a and c show the absorption spectra per bilayer for $(pLys/CdSe)_n$ and $(pLys/CdSe@CdS)_n$ films, respectively. It is clear that in both cases, the absorbance of films globally increases with the number of bilayers.

This suggests that the NPs were successfully assembled onto the film and that the number of NPs inside the film increases with the number of deposition cycles. The absorption spectra of CdSe and CdSe@CdS NPs in the multilayer films are similar to those of CdSe and CdSe@CdS NPs dispersed in water, which indicates that NPs in the film are well separated from each other and that no aggregation takes place during the assembling processes. Furthermore, the absorbance of the films increases linearly with the number of bilayers, as illustrated in Figure 1b for absorbances of CdSe NPs at 442 and 540 nm, and in Figure 1d for absorbances of CdSe@CdS NPs at 440 and 530 nm. This good linearity indicates a uniform deposition process for each assembling cycles up to 10 bilayers. The nanostructure characterization of this kind of films has been extensively studied by a variety of spectroscopic techniques as well as SEM, AFM, Kelvin probe, conductivity, and electrochemical techniques.[20–22,27,28] The MUA layer thickness was found to be approximately 2 to 3 nm,[21] the average pLys layer thickness is between 2.5 and 5 nm.[20,21]

Figure 2a displays and compares the steady-state fluorescence spectra of CdSe NPs in solution and in the multilayer films. The fluorescence spectrum of the

CdSe NPs in solution features a narrow band with a bell shape in the spectral range of 500−600 nm with a maximum at 550 nm, which originates from the $1s_e−1s_h$ excitonic transitions. Identical emission spectra can be observed for the $(pLys/CdSe)_n$ multilayer films. The fluorescence intensity also increases linearly with the number of pLys/CdSe units (inset of Figure 2a), which further confirms the uniformity obtained for each assembling cycle. Similar behavior is observed for $(pLys/CdSe@CdS)_n$, where a strong fluorescence with an emission maximum at 540 nm is observed (Figure 2b).

The relative intensity of the emission was also found to increase linearly with increasing the number of bilayers. This kind of layer-by-layer assemblies has recently
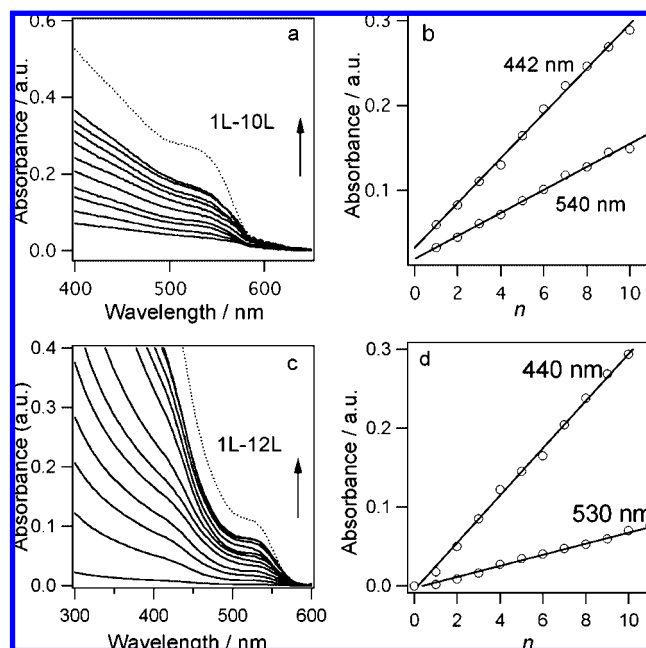

Figure 1. UV−vis absorption spectra of alternating film deposition of $(pLys/CdSe)_n$ bilayers (a) and $(pLys/CdSe@CdS)_n$ bilayers (c). The dotted lines in panels a and c represent the absorption spectra of CdSe and CdSe@CdS dispersions in aqueous solutions, respectively. Shown are the absorbances at the indicated wavelengths *vs* the number of bilayers *n* of CdSe (b) and CdSe@CdS (d). The solid lines correspond to the linear fittings.

TABLE 1. Fluorescence Decay Fit Parameters for the NPs in Solution and for Different Number of Layers of (pLys/CdSe)$_n$ and (pLys/CdSe@CdS)$_n$

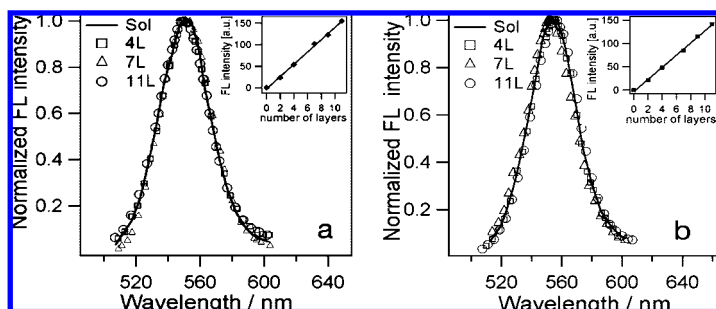|	A_1	τ_1 (ns)	A_2	τ_2 (ns)	A_3	τ_3 (ns)	$\sum A_i\tau_i$ (ns)	χ^2
CdSe NP	17%	0.61	34%	3.23	49%	17.23	9.64	1.26
(pLys/CdSe)$_4$	10%	0.94	33%	3.23	57%	21.67	13.51	1.31
(pLys/CdSe)$_7$	9%	0.97	32%	4.58	59%	19.3	12.92	1.20
(pLys/CdSe)$_{11}$	9%	1.08	32%	5.28	59%	22.28	14.93	1.23
CdSe@CdS NP	35%	0.51	27%	4.2	38%	25.44	10.96	1.18
(pLys/CdSe@CdS)$_{11}$	28%	0.97	30%	6.87	42%	29.3	14.63	1.22

Figure 2. Steady-state fluorescence spectra of CdSe (a) and CdSe@CdS (b) QDs in films at n = 4, 7, and 11. The solid lines represent the emission in solution. The insets show the emission intensity vs the number of bilayers.

found many applications like patterning[29] and data storage[30] in QD films.

Charge Carrier Dynamics of (pLys/CdSe)$_n$ and (pLys/CdSe@CdS)$_n$ Films. Time-resolved fluorescence measurements provide a highly sensitive method to probe the charge transfer kinetical properties of the particles. These measurements were here performed using a TCSPC setup. In contrast to steady-state fluorescence experiments that showed no differences between bulk and film emission spectra, CdSe and CdSe@CdS NPs display dif-
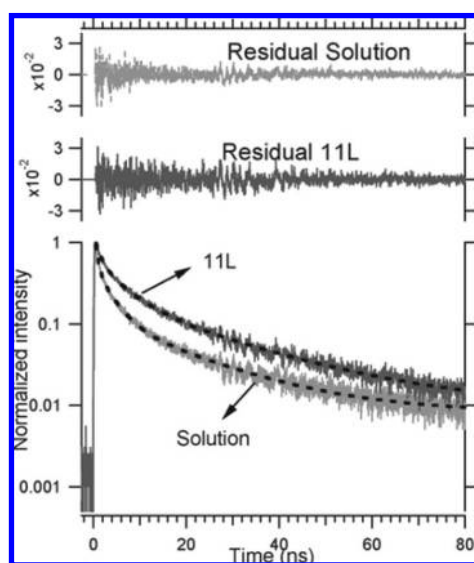
ferent charge carrier kinetics in the film compared to bulk solution, as shown in Figure 3 and Figure S3 (Supporting Information), respectively. The measurements (film and solution) were carried out exactly in the same conditions of excitation wavelength, laser power, repetition rate, and detecting wavelength. Immediately from Figure 3 and Figure S3, it can be observed that the fluorescence decay of CdSe and CdSe@CdS NPs in solution are faster than that in the multilayer film. To analyze the data, both traces were fitted by a three exponential function and the fit parameters are shown in Table 1. The fitting equation is described as follows:

$$I(t) = y_0 + a_1 \exp\left(-\frac{t}{\tau_1}\right) + a_2 \exp\left(-\frac{t}{\tau_2}\right) + a_3 \exp\left(-\frac{t}{\tau_3}\right)$$
(1)

τ_1, τ_2, and τ_3 are the lifetime constants of the fit function, while a_1, a_2, and a_3 are the pre-exponential factors and represent the amplitude of each lifetime constant. The number of components in the fit function and the best fitting values were based on minimizing the variation of the residual and on the closest value of χ^2 to 1.

To determine the relative fluorescence intensity contribution of each lifetime component to the total fluorescence intensity, we calculated the normalized percentage amplitudes A_1, A_2, and A_3 from the observed fluorescence decay times and pre-exponential factors using the following equation:

$$A_i = 100 \cdot a_i\tau_i / \sum_{i=1}^{3} a_i\tau_i$$
(2)

The fit results show some interesting trends. The fluorescence decay is best described by a multiexponential fit with three lifetime components τ_1 < 2 ns, τ_2 ≈ 3−6 ns, and τ_3 > 17 ns. All the lifetime constants are slightly larger in the film than in solution with an average lifetime varying from about 10 ns in solution to about 15 ns for a 11 bilayers film. It is also clear that increasing the number of layers does not really change the dynamics of these particles since the amplitudes of each lifetime are almost stable.

The explanation of the origin of each lifetime component is outside the scope of the present work. Several groups have tried to provide a physical interpretation of fluorescence lifetime of various semiconducting NPs (CdSe, CdS, CdTe, GaSe, CdSe@ZnS, CdSe@CdS, . . .) measured using different methods (multiexponentials, stretched exponential, or both together) according to the time window studied.[31−45] To date, no detailed physical model has been used to describe their emission dynamics. Consequently, we will present only a brief qualitative discussion of each parameter. The shortest lifetime τ_1 is probably due to the rapid quenching by various surface states.[31,32,46] However, the na-

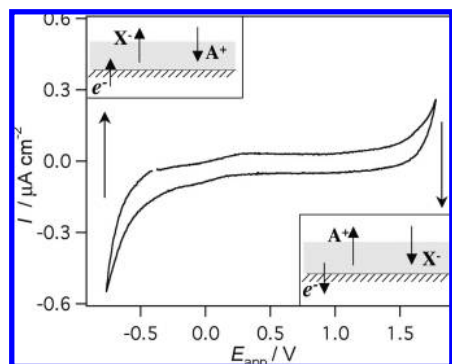
Figure 3. Fluorescence decay profiles of CdSe in solution and in (pLys/CdSe)$_{11}$. The dashed lines show the best fit obtained by eq 1. The curves in the upper panels represent the plots of the weighted residuals for three-exponential fittings.

Figure 4. Cyclic voltammetric response of a (pLys/CdSe)$_7$ at a scan rate of 10 mV s^{-1}.

ture of these surface states is not completely clear as they depend on the synthesis route. Here, the citric acid layer is likely to be involved. As τ_1 is smaller in the bulk (NPs in solution) compared to the film, but independent of the film thickness, the electrostatic interactions between the citrate coated NPs and pLys could be at the origin of the reduction of the number of the surface states, leading to the longer lifetime in the film due to the change of the local electric field. This dynamic component plays a larger role in solution than in the film, and this accounts partly for the variation of the average lifetime value. One can speculate that pH may be the cause for this variation, as pLys is likely to increase the film pH, thereby neutralizing the citric acid ligands and decreasing the number of surface traps.

The second lifetime τ_2 has been previously attributed to the lifetimes of charged excitons (trions) for charged particles like here the negatively charged CdSe and CdSe@CdS NPs.[31,35,36] It can be observed that τ_2 hardly varies with the environment and can be considered as an intrinsic property of the NP. The longest lifetime τ_3 has been shown previously[31,33,36,40,41] to be independent from the excitation power and from any chemical treatment or surface modifications, supporting the fact that τ_3 is an intrinsic property of the particle. The present data show that τ_3 does not increase with the film thickness, although a difference can be observed between the bulk and the film. This third term also accounts partly for the average lifetime difference between the bulk and the film.

All in all, we can unambiguously conclude that films of different thicknesses of (pLys/CdSe)$_n$ and (pLys/CdSe@CdS)$_n$ incorporate nanoparticles having similar charge carrier dynamics for different film

thicknesses larger than three layers, showing that the films behave uniformly.

Photocurrent Responses of (pLys/CdSe)$_n$ and (pLys/CdSe@CdS)$_n$ Films. Figure 4 shows the cyclic voltammetric response of a (pLys/CdSe)$_7$ film in a DCE electrolyte solution containing 5 mM BTPPATPFB, recorded in the dark at a scan rate of 10 mV · s^{-1}. A potential window from −0.5 to 1.5 V was obtained, in which mainly a capacitive background current was observed, allowing the study of the photoelectrochemical response of CdSe.[24] When an aqueous film thicker than 20 nm, that is, composed of more than three bilayers is immersed into the organic electrolyte, we form two polarized interfaces in series, namely, the electrode/aqueous film interface where only electron transfer reactions can take place and the aqueous film/organic solution interface where both heterogeneous electron transfer reactions and ion transfer reactions can occur. These two interfaces in series result in a large potential window being the sum of two independent potential windows.

The electron transfer at the gold electrode must be accompanied by a complementary charge transfer process between the film and the solution in order to maintain the electroneutrality of the film: at positive potentials, the anodic oxidation at the electrode is equilibrated, in the absence of redox reactions at the liquid | liquid interface, either by the ingress of anions from the organic phase into the film or by the egress of
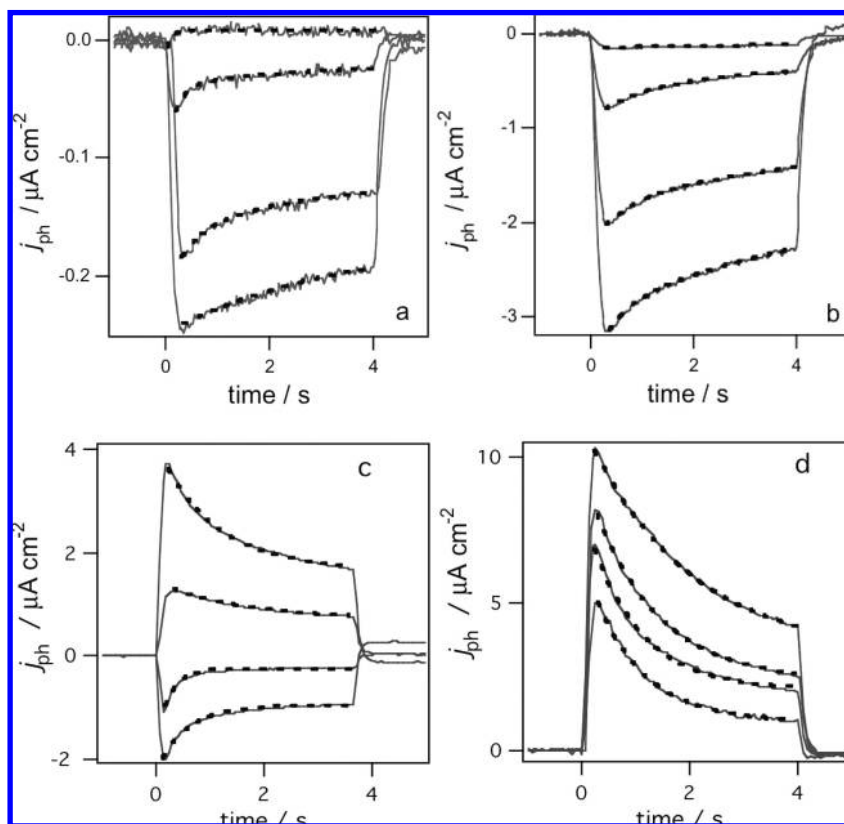

Figure 5. Photocurrent transient responses of (pLys/CdSe)$_1$ (a), (pLys/CdSe)$_7$ (b), (pLys/CdSe@CdS)$_1$ (c), and (pLys/CdSe@CdS)$_7$ (d) at four different potentials: −0.4, 0, 0.4, and 0.8 V from bottom to top. The dashed lines are fittings employing eq 7.
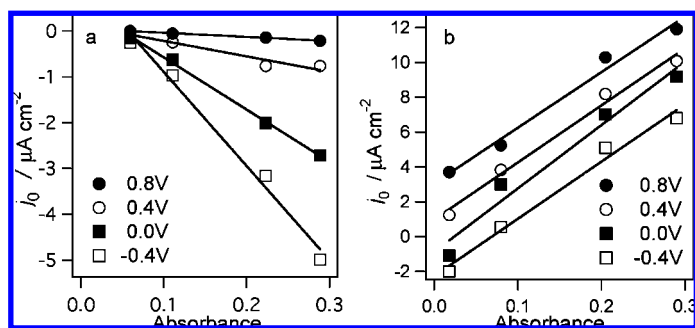
Figure 6. The initial photocurrent of (pLys/CdSe)$_n$ (a) and (pLys/CdSe@CdS)$_n$ (b) as a function of the absorbance at different applied potentials.

the cations. On the other hand, at negative potentials, the electroneutrality is maintained either by the ingress of cations or the egress of anions.

Figure 5 panels a and b display the photocurrent transients at various potentials obtained for films with different numbers of bilayers (pLys/CdSe)$_n$. It is clear that the photocurrent strongly depends on the number of bilayers and on the applied potential. Except for a small photoanodic current observed at very positive potentials for a thin film, as shown in Figure 5a, mainly photocathodic currents were obtained. The photocurrent transients have almost the same shape, regardless of the number of layers, rising sharply to a maximum initial value j_0 upon illumination and decaying slowly in the following seconds. When the illumination is stopped, the photocurrent decreases back to zero.

In the general case, the initial photocurrent is only associated with the photo-oxidation and photoreduction of the film and it can be simply expressed by[17]

$$j^0_{ph} = \Phi(k^*_{ox} - k^*_{red}) \qquad (3)$$

where k^*_{ox} and k^*_{red} are the respective electron transfer rate constants (s^{-1}) from the excited film to the gold surface (photo-oxidation) or from the gold electrode to the excited film (photoreduction) as illustrated in Scheme 2.

Φ is defined by

$$\Phi = \frac{FAI_0}{N_A k_r} \qquad (4)$$

where F, A, I_0 and N_A denote Faraday's constant, the absorbance of the film, the incident light intensity, and Avogadro's constant, respectively; k_r is the average rate constant assigned to the decay of the excited-state of CdSe particles as measured by TCSPC. When only a photocathodic current is observed, the photoreduction is dominant and we have $k^*_{red} > k^*_{ox}$. In this case, eq 3 reduces to

$$j^0_{ph} = -\Phi k^*_{red} = -\frac{FI_0 k^*_{red}}{N_A k_r}A \qquad (5)$$

Equation 5 predicts that the initial photocurrent under these conditions is proportional to the absorbance of the film and to the rate constant k^*_{red}. The dependence of the initial photocurrent on the number of pLys/CdSe bilayers and therefore on the absorbance of the film is demonstrated in Figure 6a. The photocathodic current increases linearly with the film thickness and the absorbance showing that all the CdSe NPs are photoelectrochemically active.

Figure 6a also illustrates that the photocurrent strongly depends on the overall potential difference applied between the gold electrode and the organic electrolyte solution. The cathodic photocurrent responses increase when the applied potential is biased to more negative values, suggesting that the rate of electron transfer from the electrode to the CdSe NPs increases. These data also clearly indicate that electron transfer or electron hopping between the NPs is a process much faster than the chemical reduction step ($k^*_{red} \gg k^*_d$). Figure 7a displays the potential dependence of k^*_{red} obtained from eq 5 for various film thicknesses, the more cathodic the faster the rate of the electron transfer reaction. The value of the incident photon to current conversion efficiency (IPCE) obtained for this system is ~0.1% for a film (pLys/CdSe)$_{10}$ at −0.4 V.

Figure 5 panels c and d represent the photocurrent responses obtained in DCE for different number of bilayers of (pLys/CdSe@CdS)$_n$ at various applied potentials. Unlike the (pLys/CdSe)$_n$ films, mainly photoanodic current were recorded, even at very negative applied potentials as soon as the film thickness was larger than three layers. It is clear that the photocurrent magnitude shows a strong dependence on the applied potential. A clear feature in these results is the increase of the photocurrent magnitude with increasing applied potentials. As can be seen in Figure 6b, the initial photocurrent of (pLys/CdSe@CdS)$_n$ is proportional to the absorbance for thick films. However, the behavior of a CdSe@CdS monolayer shows two mechanisms; photocathodic at negative potentials and photoanodic at positive potentials. As a result, the absorbance dependence of the initial photocurrent is offset by the behavior of the first layer. For thick films, when only a photoanodic current is observed, we have $k^*_{ox} \gg k^*_{red}$ and eq 3 can be reduced to
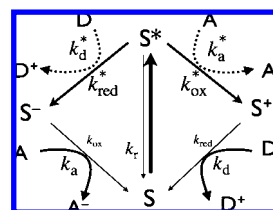
Scheme 2. Schematic representation of the photoinduced electron transfer reactions. S represents the sensitizer (CdSe or CdSe@CdS particles), D is an electron donor, and A is an electron acceptor.

$$j_{ph}^0 = \Phi k_{ox}^* = \frac{F I_0 k_{ox}^*}{N_A k_r} A \qquad (6)$$

Knowing the initial photocurrents and the absorbance for each number of bilayers, the values of k_{ox}^* can be extracted from eq 6. As can be seen in Figure 7b, k_{ox}^* increases when increasing the applied potential to more positive values. Except for the first three layers, k_{ox}^* is independent of the film thickness.

Kinetic Model. To analyze the kinetics of photoinduced processes and coupled reactions at a film-coated electrode, the model illustrated in Scheme 2 was used to derive the time response of the photocurrent:[17]

$$j_{ph} = \Phi(\alpha + \beta e^{-(k_{ox}+k_a)t} + \gamma e^{-(k_{red}+k_d)t}) \qquad (7)$$

with the coefficients α, β, and γ relative to the steady-state, cathodic, and anodic photocurrents given respectively by

$$\alpha \approx (k_{ox}^* - k_{red}^*) - \beta - \gamma \qquad (8)$$

$$\beta \approx -k_{ox}(k_{red}^* + k_d^*)/(k_{ox} + k_a) \qquad (9)$$

$$\gamma \approx k_{red}(k_{ox}^* + k_a^*)/(k_{red} + k_d) \qquad (10)$$

where k_a^* (s^{-1}) denotes the rate constant for the excited NP quenching by an electron acceptor in the film and k_d^* (s^{-1}) represents the rate constant for the quenching by an electron donor present in the film. k_{ox} and k_{red} are the respective rate constants (s^{-1}) for the back electron transfer to the electrode, and k_a and k_d are the rate constants for the chemical recycling pathway. The first term in eq 7 describes the steady state photocurrent. The second and the third terms represent the photocurrent decay in the case of cathodic and anodic photocurrent, respectively. Here, in the case of (pLys/CdSe)$_n$, the initial photocurrent is mainly determined by k_{red}^*, and the photocurrent decay corresponds to the second term of eq 7 and is associated with the back electron transfer to the electrode k_{ox} and the rate of electron transfer k_a between the reduced NPs and an electron acceptor in the film. Exponential fittings of the photocurrent transients yielding $k_{ox} + k_a$ are shown as dashed curves in Figure 5a,b showing clearly that this equation provides an adequate estimation of the photocurrent kinetics. The potential dependence of $k_{ox} + k_a$ for various film thicknesses was a decrease with increasing potentials, as shown in Figure S6 (Supporting Information). As one would expect k_{ox} to increase with increasing potentials, we can conclude that the dominating factor is here k_a, that is, the reoxidation of the film by an electron acceptor. Considering that no pho-
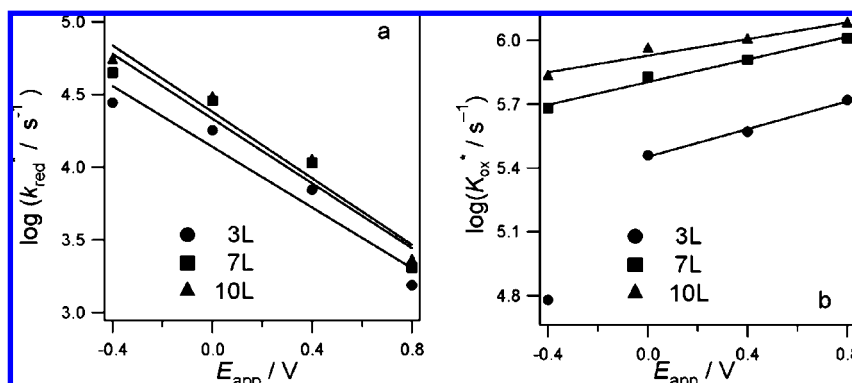

Figure 7. Rate constant k_{red}^* (a) and k_{ox}^* (b) as function as of applied potentials. The values were obtained by linear fittings of Figure 6a and Figure 6b, respectively.

tocurrents can be observed when the organic electrolyte is purged with argon, one can speculate that the film is reoxidized by molecular oxygen that has a concentration in the millimolar range in 1,2-dichloroethane. We can conclude that upon irradiation, the (pLys/CdSe)$_n$ films act as a photocathode for oxygen reduction. It is also important to notice that no photocurrent responses are observed when the films are in aqueous solutions, as the film is not stable in water and decomposes after a short time.

The photocurrent decay of photoanodic currents is given by the third term of eq 7 and is associated with the sum of the rate constant k_{red} for the back electron transfer to the electrode and the rate constant k_d for the rereduction of the oxidized film by an electron donor in the film. Fittings of the photocurrent transients employing eq 7 are shown as dashed curves in Figure 5c,d. The potential dependence for the $k_{red} + k_d$ values shows an increase with increasing potentials, as represented in Figure S7 (Supporting Information) for 3, 7, and 10 bilayers of (pLys/CdSe@CdS)$_n$. Again as one would expect k_{red} to decrease upon going anodic, we can conclude that the limiting step here is the reduction of the oxidized film. The electrode then behaves as a photoanode. In the absence of added electron donor, it is possible that water is oxidized to oxygen.

From a mechanistic viewpoint, we can postulate in the case of CdSe NPs that electron traps located close to the conduction band of the CdSe nanoparticles may be involved to trap the excited electrons, leading to an electron transfer from the Fermi level of the gold electrode to the valence band of the NPs. The reduced NPs may then be recycled by an electron acceptor in the film or in the organic phase, for example, here by oxygen. We have demonstrated in a previous communication the difference between an aqueous polymer-film-modified electrode in an organic electrolyte solution and a solid-electrode-supported ITIES (interface between two immiscible electrolyte solutions). In the former case, the film was thinner than five bilayers of pLys/pGlu pairs, that is, 20 nm, and the potential drop occurs all through the film. In the latter case, the film
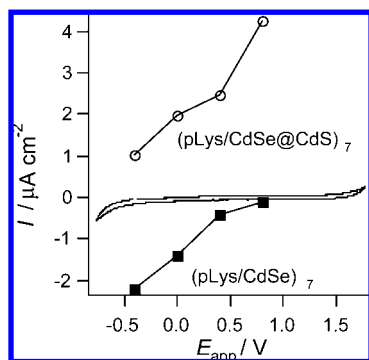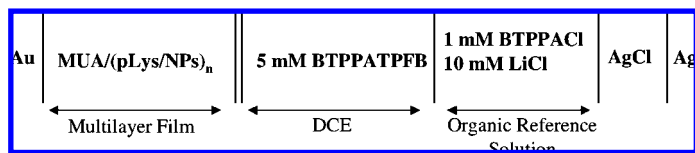
Figure 8. Current—voltage response in dark and under illumination for (pLy/NPs)$_7$

was thicker and the potential drop was found to occur both at the gold/film interface and the film/organic electrolyte interface. The fact that here k_a is found to exhibit a similar potential dependence for thick films suggests that the oxygen reduction may occur principally at the film/organic electrolyte interface. For thinner films, the electrode behaves as a polymer-modified electrode.

In the case of CdSe@CdS NPs, the presence of a CdS shell around the CdSe core changes the nature of the trapped state. From the present results, we can speculate the presence of hole traps near the valence band of the NPs. Upon irradiation, the NPs can inject electrons from the conduction band to the Fermi level of the gold electrode. These oxidized NPs can then be rereduced by electron donors present in the film.

Figure 8 illustrates photocurrents sampled after 4 s for both, (pLys/CdSe)$_n$ and (pLys/CdSe@CdS)$_n$ films. The former behaves as a nanoporous bulk photocath-

Scheme 3. Schematic illustration of the electrochemical cell and electrolyte compositions.

ode able to reduce oxygen, whereas the latter behaves as a nanoporous photoanode able to oxidize water. It is interesting to notice that the two types of films have roughly the same absorbance at the photocurrent excitation wavelength of 442 nm, and as the consequence the range of photocurrents measured is similar. If a (pLys/CdSe)$_n$ and a (pLys/CdSe@CdS)$_n$ cell were mounted in series and biased at zero volt, Figure 8 suggests that the system could produce a couple of microamps per cm^2.

CONCLUSIONS

Thin photoactive films composed of positively charged pLys and negatively charged CdSe and CdSe@CdS NPs were fabricated by layer-by-layer assembly on a carboxylic acid terminated alkanethiol-modified gold electrode. UV—vis absorption and fluorescence spectroscopic measurements reveal a linear increase of NP absorbance with the number of adsorbed layers, indicating a uniform film formation. Fluorescence lifetime measurements using TCSPC technique show that the fluorescence decay of the NPs in the multilayer films is slightly different with that in solution, but similar regardless of the film thickness. Photocathodic currents responses of the multilayer CdSe film were measured as a function of the applied potential and the number of adsorbed CdSe layers. On the other hand, large photoanodic currents were obtained when the CdSe particles are replaced by CdSe@CdS NPs. The photocathodic and photoanodic currents were correlated to reoxidation and rereduction of the film. A kinetic model and simulations show similar electron rate constants when the films are composed of more than three layers. These data suggest that the semiconductor film behaves as one electronic unit, that is, like a nanoporous photocathode when using CdSe particles and nanoporous photoanode when using CdSe@CdS core—shells. Finally, we found that these NPs are electronically coupled and that electron transfer between them is a fast process compared to the electrochemical step at the electrode.

EXPERIMENTAL SECTION

Chemicals. All reagents were used as received. Poly-L-lysine (pLys; MW = 30300)) was purchased from Sigma. 11-Mercaptoundecanoic acid (MUA) was obtained from Aldrich. Disodium hydrogen phosphate (Na$_2$HPO$_4 \cdot$ 2H$_2$O), sodium dihydrogen phosphate (NaH$_2$PO$_4 \cdot$ H$_2$O), and bis(triphenylphosphoranylidene) ammonium chloride (BTPPAC1) are Fluka products. Lithium tetrakis(pentafluorophenyl) borate (LiTPFB) was bought from Boulder Scientific. 1,2-Dichloroethane (DCE, Aldrich) and ethanol (Aldrich) were used as solvents. The supporting electrolyte in the organic phase was BTPPATPFB, which was prepared as previously reported.[47] All aqueous solutions were prepared with purified water from a Milli-Q 185 system. Finally, citrate-stabilized CdSe and CdSe@CdS nanoparticles were prepared following the protocol reported previously using a 4:1 Cd/Se molar ratio.[48] The obtained CdSe and CdSe@CdS nanoparticles have

an average size around 2.5 to 3 nm as determined by transmission electron microscopy.

Film Preparation. The preparation of gold electrodes was carried out by evaporation on a glass substrate. The gold layers were initially modified with a monolayer of MUA by immersion into an ethanolic solution of 1 mM MUA for 12 h. Loosely bound MUA molecules were removed from the surface by rinsing successively with ethanol and water before drying the electrode under an argon stream. The preparation of pLys/NPs multilayer films is based on the electrostatic self-assembly, dipping sequentially the MUA-modified gold electrode into an aqueous 1 g · L^{-1} of pLys prepared in a phosphate buffer at pH 8.4 for 15 min and an aqueous dispersion of CdSe or CdSe@CdS for 1 h. Between each dip, the surface was rinsed with Millipore water and blown dry under an argon stream. The multilayer films prepared by repeating this dipping cycle n times is designated (pLys/

CdSe)$_n$ when using CdSe particles and (pLys/CdSe@CdS)$_n$ when using CdSe@CdS core/shells.

Spectroscopic Measurements. The UV−visible absorption measurements were performed on an Ocean Optics CHEM2000 UV−vis spectrophotometer. The steady state and time-resolved fluorescence measurements were performed using the time-correlated single photon counting (TCSPC) technique. For this purpose, multilayers of pLys and NPs were grown on microscope glass slides previously treated with a piranha solution (piranha solution is very energetic and potentially explosive; handle it with care) in the absence of the gold/MUA layer. Femtosecond laser pulses of 80 MHz, tunable from 700−1000 nm from a mode locked Ti:sapphire laser (Spectra Physics, Tsunami), pumped by a Nd:YVO$_4$ solid state laser (Spectra Physics, Millennia Xs), were directed to a pulse picker and frequency doubler (Spectra Physics, model 3980). For the present study, the repetition rate of the optical pulses was set at 400 kHz. The excitation laser beam was s-polarized using a polarizer. The fluorescence was focused by a lens placed at a 90° angle from the excitation beam to the entrance slit of a monochromator (Jobin Yvon, H-10) and detected by a cooled microchannel plate photomultiplier (MCP-PM, Hamamatsu, R3809U-50). The temperature of the MCP-PM housing was set at −20 °C to minimize the dark counts from the MCP-PM. The output of the MCP-PM was further amplified using an amplifier (Becker & Hickl GmbH) and analyzed by a single photon counting module (Edinburgh Instruments, TCC900). The constant fraction discriminator (CFD) parameters were optimized using T900 software to get the best fit and lifetimes for the fluorescence lifetime standard molecules. The overall instrumental response function, as recorded by scattering the excitation light using Ludox in a sample cell, was around 60 ps full width at half-maximum (fwhm) for 100 ns as a temporal window. The laser pulse STOP synchronization was performed by using the laser fundamental beam from the pulse picker and detected using an optical trigger OT900 (15 V bias, risetime 450 ps). The fluorescence detecting wavelength was set at 550 nm throughout the study. The number of fluorescent photons was kept low relative to the number of start pulses (1% or less).

Electrochemical and Photocurrent Measurements. The electrochemical cell used in all measurements is a custom built three-electrode cell with a cylindrical glass vessel. The multilayer-modified gold slide functions as the working electrode, with a Pt wire counter electrode and an Ag/AgCl reference electrode. The junction between the reference electrode and the organic electrolyte was established by an aqueous solution containing 10 mM LiCl and 1 mM BTPPACl as indicated in Scheme 3. The DCE phase contained 5 mM of BTPPATPFB as supporting electrolyte in order to obtain a large polarization window at the water/DCE interface. The potential supplied by a wave function generator (Standford Research System, S335) was applied to the electrochemical cell by a custom built potentiostat.

Photocurrent measurements were performed under potentiostatic conditions with potentials supplied by a Hi-Tek wave function generator. The illumination is provided by the 442 nm beam line of a CW He−Cd laser (Omnichrome Series 74). Neutral density filters were used for controlling the photon flux. A mechanical shutter was used to control the light on and off. The photon flux was measured using a calibrated power meter (Gentec). The illumination and current recording were synchronized by means of custom built Labview programs. The spot size of the laser beam was 3 mm in diameter, and the photocurrent density was calculated using the surface area of the gold substrate.

Supporting Information Available: AFM images of the ultrathin film, TEM images of CdSe particles, additional kinetic studies, steady-state emission, fluorescence lifetime and photocurrent transient of NPs. This information is available free of charge *via* the Internet at http://pubs.acs.org.

REFERENCES AND NOTES

1. Alivisatos, A. P. Semiconductor Clusters, Nanocrystals, and Quantum Dots. *Science* **1996**, *271*, 933–937.
2. Woggon, U. *Optical Properties of Semiconductor Quantum Dots*; Tracts in Modern Physics; Springer: New York, 1997.
3. Nirmal, M.; Brus, L. Luminescence Photophysics in Semiconductor Nanocrystals. *Acc. Chem. Res.* **1999**, *32*, 407–414.
4. Murphy, C. J.; Coffer, J. L. Quantum Dots: A Primer. *Appl. Spectrosc.* **2002**, *56*, 16A−27A
5. Klimov, V. I. Nanocrystal Quantum Dots: From Fundamental Photophysics to Multicolor Lasing. *Los Alamos Science* **2003**, *28*, 214–220.
6. Su, B.; Fermin, D. J.; Abid, J.-P.; Eugster, N.; Girault, H. H. Adsorption and Photoreactivity of CdSe Nanoparticles at Liquid|Liquid Interfaces. *J. Electroanal. Chem.* **2005**, *583*, 241–247.
7. Cottingham, K. Quantum Dots: Leave the Light On. *Anal. Chem.* **2005**, *77*, 354A–357A
8. Tian, Y.; Wu, C.; Fendler, J. H. Fluorescence Activation and Surface-State Reactions of Size-Quantized Cadmium Sulfide Particles in Langmuir-Blodgett Films. *J. Phys. Chem.* **1994**, *98*, 4913–4918.
9. Torimoto, T.; Tsumura, N.; Miyake, M.; Nishizawa, M.; Sakata, T.; Mori, H.; Yoneyama, H. Preparation and Photoelectrochemical Properties of Two-Dimensionally Organized CdS Nanoparticle Thin Films. *Langmuir* **1999**, *15*, 1853–1858.
10. Colvin, V. L.; Goldstein, A. N.; Alivisatos, A. P. Semiconductor Nanocrystals Covalently Bound to Metal Surfaces with Self-Assembled Monolayers. *J. Am. Chem. Soc.* **1992**, *114*, 5221–5230.
11. Gao, M.; Zhang, X.; Yang, B.; Li, F.; Shen, J. Assembly of Modified CdS Particles/Cationic Polymer Based on Electrostatic Interactions. *Thin Solid Films* **1996**, *284−285*, 242–245.
12. Kotov, N. A.; Dekany, I.; Fendler, J. H. Layer-by-Layer Self-Assembly of Polyelectrolyte-Semiconductor Nanoparticle Composite Films. *J. Phys. Chem.* **1995**, *99*, 13065–13069.
13. Ogawa, S.; Fan, F.-R. F.; Bard, A. J. Scanning Tunneling Microscopy, Tunneling Spectroscopy, and Photoelectrochemistry of a Film of Q-CdS Particles Incorporated in a Self-Assembled Monolayer on a Gold Surface. *J. Phys. Chem.* **1995**, *99*, 11182–11189.
14. Lvov, Y.; Ariga, K.; Onda, M.; Ichinose, I.; Kunitake, T. Alternate Assembly of Ordered Multilayers of SiO$_2$ and Other Nanoparticles and Polyions. *Langmuir* **1997**, *13*, 6195–6203.
15. Decher, G.; Eckle, M.; Schmitt, J.; Struth, B. Layer-by-Layer Assembled Multicomposite Films. *Curr. Opin. Colloid Interface Sci.* **1998**, *3*, 32–39.
16. Nakanishi, T.; Ohtani, B.; Shimazu, K.; Uosaki, K. Layer-by-Layer Self-Assembly of Composite Films of CdS Nanoparticle and Alkanedithiol on Gold: An X-Ray Photoelectron Spectroscopic Characterization. *Chem. Phys. Lett.* **1997**, *278*, 233–237.
17. Hojeij, M.; Eugster, N.; Su, B.; Girault, H. H. CdSe Sensitized Thin Aqueous Films: Probing the Potential Distribution Inside Multilayer Assemblies. *Langmuir* **2006**, *22*, 10652–10658.
18. Cheng, Y.; Murtomaki, L.; Corn, R. M. Electrochemical Characterization of the Ultrathin Polypeptide Film/1,2-Dichloroethane Liquid|Liquid Interface. *J. Electroanal. Chem.* **2000**, *483*, 88–94.
19. Tan, S.; Hojeij, M.; Su, B.; Meriguet, G.; Eugster, N.; Girault, H. H. 3d-Ities Supported on Porous Reticulated Vitreous Carbon. *J. Electroanal. Chem.* **2007**, *604*, 65–71.
20. Carrara, M.; Kakkassery, J. J.; Abid, J.-P.; Fermin, D. J. Modulation of the Work Function in Layer-by-Layer Assembly of Metal Nanoparticles and Poly-L-Lysine on Modified Au Surfaces. *ChemPhysChem* **2004**, *5*, 571–575.

ARTICLE

21. Cheng, Y.; Corn, R. M. Ultrathin Polypeptide Multilayer Films for the Fabrication of Model Liquid/Liquid Electrochemical Interfaces. *J. Phys. Chem. B* **1999**, *103*, 8726–8731.

22. Chirea, M.; Garcia-Morales, V.; Manzanares, J. A.; Pereira, C.; Gulaboski, R.; Silva, F. Electrochemical Characterization of Polyelectrolyte/Gold Nanoparticle Multilayers Self-Assembled on Gold Electrodes. *J. Phys. Chem. B* **2005**, *109*, 21808–21817.

23. Uosaki, K.; Okamura, M.; Ebina, K. Photophysical and Photoelectrochemical Characteristics of Multilayers of CdS Nanoclusters. *Faraday Discuss.* **2003**, *125*, 39–53.

24. Hickey, S. G.; Riley, D. J. Photoelectrochemical Studies of CdS Nanoparticle-Modified Electrodes. *J. Phys. Chem. B* **1999**, *103*, 4599–4602.

25. Halaoui, L. I. Photoelectrochemistry in Aqueous Media at Polyacrylate-Capped Q-CdS Assembled in Polyelectrolyte Matrix on Electrode Surfaces. *J. Electrochem. Soc.* **2003**, *150*, E455−E460.

26. Halaoui, L. I. Layer-by-Layer Assembly of Polyacrylate-Capped CdS Nanoparticles in Poly(diallyldimethylammonium chloride) on Solid Surfaces. *Langmuir* **2001**, *17*, 7130–7136.

27. Zhao, J.; Bradbury, C. R.; Huclova, S.; Potapova, I.; Carrara, M.; Fermin, D. J. Nanoparticle-Mediated Electron Transfer Across Ultrathin Self-Assembled Films. *J. Phys. Chem. B* **2005**, *109*, 22985–22994.

28. Tang, Z.; Wang, Y.; Kotov, N. A. Semiconductor Nanoparticles on Solid Substrates: Film Structure, Intermolecular Interactions, and Polyelectrolyte Effects. *Langmuir* **2002**, *18*, 7035–7040.

29. Wang, Y.; Tang, Z.; Correa-Duarte, M. A.; Liz-Marzan, L. M.; Kotov, N. A. Multicolor Luminescence Patterning by Photoactivation of Semiconductor Nanoparticle Films. *J. Am. Chem. Soc.* **2003**, *125*, 2830–2831.

30. Kimura, J.; Maenosono, S.; Yamaguchi, Y. Near-Field Optical Recording on a CdSe Nanocrystal Thin Film. *Nanotechnology* **2003**, *14*, 69–72.

31. Al Salamn, A. Spectroscopy and Kinetic Studies of Electron-Hole Recombination in CdSe Nanoparticles: Effect of Size, Shape, and Lattice Structure. Ecole Polytechnique Fédérale de Lausanne (EPFL): Lausanne, Switzerland, 2007.

32. Lakowicz, J. R. Time-Resolved Laser Spectroscopy in Biochemistry. *Proc. Int. Soc. Opt. Eng.* **1990**, *13*, 1024.

33. Bawendi, M. G.; Carroll, P. J.; Wilson, W. L.; Brus, L. E. Luminescence Properties of CdSe Quantum Crystallites−Resonance between Interior and Surface Localized States. *J. Chem. Phys.* **1992**, *96*, 946–954.

34. Bruchez, M.; Moronne, M.; Gin, P.; Weiss, S.; Alivisatos, A. P. Semiconductor Nanocrystals as Fluorescent Biological Labels. *Science* **1998**, *281*, 2013–2016.

35. Califano, M.; Franceschetti, A.; Zunger, A. Temperature Dependence of Excitonic Radiative Decay in CdSe Quantum Dots: The Role of Surface Hole Traps. *Nano Lett.* **2006**, *5*, 2360–2364.

36. Javier, A.; Magana, D.; Jennings, T.; Strouse, G. F. Nanosecond Exciton Recombination Dynamics in Colloidal CdSe Quantum Dots under Ambient Conditions. *Appl. Phys. Lett.* **2003**, *83*, 1423–1425.

37. Labeau, O.; Tamarat, P.; Lounis, B., Temperature Dependence of the Luminescence Lifetime of Single CdSe/Zns Quantum Dots. *Phys. Rev. Lett.* **2003**, *90*.

38. Li, L. S.; Hui, Z.; Chen, Y. M.; Zhang, X. T.; Peng, X. G.; Liu, Z. F.; Li, T. J. Preparation and Organized Assembly of Nanoparticulate Tio2-Stearate Alternating Langmuir-Blodgett Films. *J. Colloid Interface Sci.* **1997**, *192*, 275–280.

39. Murray, C. B.; Norris, D. J.; Bawendi, M. G. Synthesis and Characterization of Nearly Monodisperse CdE (E = S, Se, Te) Semiconductor Nanocrystallites. *J. Am. Chem. Soc.* **1993**, *115*, 8706–8715.

40. Nirmal, M.; Murray, C. B.; Bawendi, M. G. Fluorescence-Line Narrowing in CdSe Quantum Dots-Surface Localization of the Photogenerated Exciton. *Phys. Rev. B* **1994**, *50*, 2293–2300.

41. Norris, D. J.; Bawendi, M. G. Structure in the Lowest Absorption Feature of CdSe Quantum Dots. *J. Chem. Phys.* **1995**, *103*, 5260–5268.

42. Wang, X. Y.; Qu, L. H.; Zhang, J. Y.; Peng, X. G.; Xiao, M. Surface-Related Emission in Highly Luminescent CdSe Quantum Dots. *Nano Lett.* **2003**, *3*, 1103–1106.

43. Zhang, J. Y.; Wang, X. Y.; Xiao, M. Modification of Spontaneous Emission from CdSe/CdS Quantum Dots in the Presence of a Semiconductor Interface. *Opt. Lett.* **2002**, *27*, 1253–1255.

44. Kloepfer, J. A.; Bradforth, S. E.; Nadeau, J. L. Photophysical Properties of Biologically Compatible CdSe Quantum Dot Structures. *J. Phys. Chem. B* **2005**, *109*, 9996–10003.

45. Schlegel, G.; Bohnenberger, J.; Potapova, I.; Mews, A. Fluorescence Decay Time of Single Semiconductor Nanocrystals. *Phys. Rev. Lett.* **2002**, *88*, 137401/137401−137401/137404.

46. Landes, C.; Burda, C.; Braun, M.; El-Sayed, M. A. Photoluminescence of CdSe Nanoparticles in the Presence of a Hole Acceptor: *N*-Butylamine. *J. Phys. Chem. B* **2001**, *105*, 2981–2986.

47. Fermin, D. J.; Dung Duong, H.; Ding, Z.; Brevet, P. F.; Girault, H. H. Photoinduced Electron Transfer at Liquid/Liquid Interfaces Part II. A Study of the Electron Transfer and Recombination Dynamics by Intensity Modulated Photocurrent Spectroscopy (IMPS). *Phys. Chem. Chem. Phys.* **1999**, *1*, 1461–1467.

48. Rogach, A. L.; Nagesha, D.; Ostrander, J. W.; Giersig, M.; Kotov, N. A. "Raisin Bun"-Type Composite Spheres of Silica and Semiconductor Nanocrystals. *Chem. Mater.* **2000**, *12*, 2676–2685.